JACS
JOURNAL OF THE AMERICAN CHEMICAL SOCIETY

Communication

pubs.acs.org/JACS

Plant Biomass Recalcitrance: Effect of Hemicellulose Composition on Nanoscale Forces that Control Cell Wall Strength

Rodrigo L. Silveira,[†,‡] Stanislav R. Stoyanov,[†,§] Sergey Gusarov,[†] Munir S. Skaf,*[,‡] and Andriy Kovalenko*[,†,∥]

[†]National Institute for Nanotechnology, 11421 Saskatchewan Drive, Edmonton, Alberta, T6G 2M9, Canada
[‡]Institute of Chemistry, State University of Campinas, Campinas, São Paulo, Brazil
[§]Department of Chemical and Materials Engineering, University of Alberta, Edmonton, Alberta, T6G 2V4, Canada
[∥]Department of Mechanical Engineering, University of Alberta, Edmonton, Alberta, T6G 2G8, Canada

Supporting Information

ABSTRACT: Efficient conversion of lignocellulosic biomass to second-generation biofuels and valuable chemicals requires decomposition of resilient plant cell wall structure. Cell wall recalcitrance varies among plant species and even phenotypes, depending on the chemical composition of the noncellulosic matrix. Changing the amount and composition of branches attached to the hemicellulose backbone can significantly alter the cell wall strength and microstructure. We address the effect of hemicellulose composition on primary cell wall assembly forces by using the 3D-RISM-KH molecular theory of solvation, which provides statistical−mechanical sampling and molecular picture of hemicellulose arrangement around cellulose. We show that hemicellulose branches of arabinose, glucuronic acid, and especially glucuronate strengthen the primary cell wall by strongly coordinating to hydrogen bond donor sites on the cellulose surface. We reveal molecular forces maintaining the cell wall structure and provide directions for genetic modulation of plants and pretreatment design to render biomass more amenable to processing.

Overcoming biomass recalcitrance constitutes the most fundamental unsolved problem of plant-based green technologies.[1,2] Plants naturally evolved to withstand harsh external mechanical, thermal, chemical, and biological factors, and so are resistant to cell wall deconstruction. Plant secondary cell walls are composed of cellulose microfibrils embedded in a complex noncellulosic matrix comprised mainly of hemicellulose and lignin. These noncellulosic components are responsible for the cohesive forces within the cell wall that entail structural support to plants.[3] Current technological applications demand decomposition of this resilient structure to extract cell wall components for production of second-generation biofuels and other valuable chemical commodities. It is well-known that cell wall recalcitrance varies among plant species and even within different phenotypes of the same plant. The close relation between recalcitrance and the chemical composition of the noncellulosic matrix suggests that cell wall strength could be tuned by carefully controlling the matrix composition.[1,3−5] Thus, full understanding of the chemical interactions within the cell walls is fundamental to gain control of the lignocellulosic biomass recalcitrance.[2]

Molecular dynamics simulations have been used to investigate decrystallization of cellulose,[6,7] the interactions between cellulose and noncellulosic components of plant cell walls,[8] and the structure and dynamics of lignin.[9] However, extremely long and costly simulations are required to obtain adequate statistical sampling addressing both solvation structure and thermodynamics of effective interactions in cell walls based on molecular forces. The 3D-RISM-KH molecular theory of solvation (three-dimensional reference interaction site model with the Kovalenko−Hirata closure approximation)[10−13] employed here bridges the gap between molecular structure and effective forces on multiple length scales. It is uniquely capable of predicting the chemistry-driven effective interactions in plant cell walls as well as enzymatic and catalytic chemical deconstruction of biomass. The method is equally applicable to nanoparticles with various surface chemistry in solutions and gels to predict such processes as aggregation and self-assembly in supramolecular cooperative interactions[14] and functionalized polymers,[15] as well as in general to complex polysaccharides, which are of great scientific and technological importance[16] because of their roles in many biochemical processes such as molecular recognition, signaling and coding.[17,18]

Glucuronoarabinoxylan, the hemicellulose type most abundant in important lignocellulosic grasses used for biofuel production, such as sugar cane and corn, consists of a xylan backbone decorated with branches of mainly glucuronic acid and arabinose, whose amount and ratio varies substantially with the plant genotype.[19] Genetic manipulation of glucuronic acid branching has been shown to significantly improve xylan extractability from cell walls without impairing plant growth.[3] High-resolution imaging indicates a strong correlation between cell wall architecture and enzymatic digestibility.[4] Here, we present a molecular view of the effective interactions between cellulose nanocrystallites (CNs) immersed in a hemicellulose hydrogel and predict the effect of hemicellulose chemical composition on the nanoscale forces that control primary cell wall assembly. To this end, we employ the statistical−mechanical, 3D-RISM-KH molecular theory of solvation,[10−13]

Received: June 5, 2013
Published: November 25, 2013

   dx.doi.org/10.1021/ja405634k | J. Am. Chem. Soc. 2013, 135, 19048−19051

summarized in the Supporting Information. This modeling approach is an important first step toward molecular level understanding of how the matrix of lignin and hemicellulose affects cell wall recalcitrance. Moreover, this methodology is capable of unraveling solvent-induced effects in cellulose deconstruction in other environments such as ionic liquids.[20]

The 3D-RISM-KH theory represents, in a single formalism, both electrostatic and nonpolar solvation features, such as hydrogen bonding, solvophobicity, structural solvent molecules, salt bridges, and other associative and steric effects. It yields the solvation structure and thermodynamics of a supramolecule in solvent mixture of a given composition in a wide range of thermo dynamic conditions, including ambient and supercritical states, nanoconfinement, solvent layering, etc. For realistic nanosystems and processes in solution, converging the 3D-RISM-KH integral equations produces accurate 3D solvation maps at far lower computational cost than molecular simulations.[21] This theory has been successfully applied to a variety of problems, in particular, self-assembly and properties of synthetic organic supramolecular nanoarchitectures,[22,23] structure and stability of oligomeric polyelectrolyte gel networks,[24] and solvation and functions of biomolecular systems, including interfacial water,[21] multilayer adsorption,[25] selective ion binding,[26] proton transport,[27] molecular recognition and ligand binding.[28]

We construct a model of a primary cell wall fragment containing two 4-chain 8-glucose-long cellulose fragments referred to as a CN immersed in aqueous solutions of the monomers arabinose, glucuronic acid and glucuronate at different concentrations. The Iβ CNs were built by using Cellulose-Builder.[29] The 3D-RISM-KH calculations are performed for hydrophilic and hydrophobic aggregation pathways of the CNs (Supporting Information, Figure S1a,b). From the interaction potentials between the species of our cell wall model, we solve the 3D-RISM-KH integral equations to yield the thermodynamics and structure of hemicellulose around CNs in terms of ensemble-averaged 3D spatial maps of site density distributions. The solvation free energy density of the hemicellulose moieties around the CNs is also obtained. The potential of mean force (PMF) between the CNs immersed in the glucuronate solutions is obtained from the 3D-RISM-KH theory as $\mathrm{PMF}(d) = u_{12}(d) + \mu_{12}(d) - \mu_1 - \mu_2$, where $u_{12}(d)$ is the interaction potential between the CNs, $\mu_{12}(d)$ is the solvation free energy of the aggregate of the CNs at separation d, and μ_1 and μ_2 are the solvation free energies of each of the CNs alone. Figure 1a,b shows the PMF for separation of the CNs along the the hydrophilic and hydrophobic pathways illustrated in Supporting Information, Figure S1a,b. The PMF for disaggregation of both face arrangement exhibits two well-defined local minima. In both cases, the first minimum at $r_{fc} \approx 0$ Å corresponds to two aggregated CNs in a direct face contact, whereas the second minimum at $r_{ss} \approx 3$ Å refers to the CNs separated by a solvent layer.

The hydrophilic face contact arrangement of the cellulose aggregate (Supporting Information, Figure S1a) is strongly stabilized because of interfibrillar hydrogen bonds and gives a global minimum of PMF. The global minimum for dissociation along the hydrophobic contact surface (Supporting Information, Figure S1b) corresponds to the solvent-separated arrangement with the CNs ≈3 Å apart and the well depth reaching ≈−7 kcal/mol in pure water. These results support the recent suggestion that CN aggregation through hydrophilic faces is preferred over the hydrophobic faces in primary cell walls.[4] Moreover, the PMF results in pure water suggest that the outer layers of a cellulose

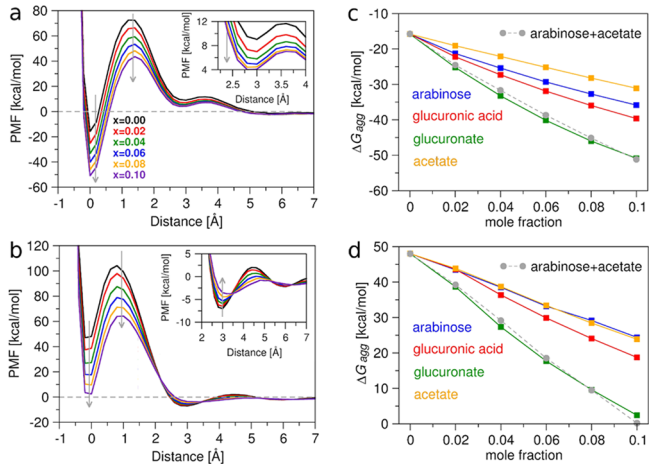

Figure 1. Potential of mean force (PMF) and aggregation free energies (ΔG_{agg}). (a) and (b): PMF along the hydrophilic and hydrophobic disaggregation pathways, respectively, at glucuronate molar fractions x = 0.0−0.1 [legend in (a)]. Grey arrows indicate PMF change with glucuronate concentration. (c) and (d): ΔG_{agg} for the hydrophilic and hydrophobic contacts, respectively, in hemicellulose hydrogels. Grey dotted line is the sum of the arabinose and acetate curves.

crystallite could be less tightly packed than the core; however, large energy barriers must be overcome to detach glucan chains from the crystallite as well as to assemble it from chains dispersed in solution.

The stability of aggregated CNs indicates how difficult it is to disrupt an arrangement within a primary cell wall. With glucuronate concentration, the face contact aggregation free energy $\Delta G_{agg} = \mathrm{PMF}(r_{fc})$ decreases as fast as the first maximum $\mathrm{PMF}(r_{bar})$, while the disaggregation barrier $\Delta G_{dis} = \mathrm{PMF}(r_{bar}) - \mathrm{PMF}(r_{fc})$ remains the same (Figure 1a). The PMF of CNs in glucuronic acid and arabinose hydrogel has a similar shape (Supporting Information, Figure S2). Thus, the larger the amount of hemicellulose, the stronger the primary plant cell wall microstructure. This is consistent with the fact that drastic structure change or absence of hemicellulose prevents plant growth because of structural collapse.[19]

Figure 1c,s shows the dependence of the aggregation free energy $\Delta G_{agg} = \mathrm{PMF}(r_{fc})$ on the hemicellulose composition and concentration and highlights the strong specific interactions between hemicellulose monomers and cellulose. Glucuronate (with a hydronium counterion, modeled after ref 26) causes the strongest stabilization of the CN aggregate, twice as strong as either arabinose or glucuronic acid. For the hydrophobic face contact (Supporting Information, Figure S1b), the stabilization due to glucuronate reaching 0.1 mole fraction leads to $\Delta G_{agg} \approx 0$, making aggregation almost spontaneous. The same trends are observed for the hydrophilic face contact (S1a), where the aggregation well deepens from $\Delta G_{agg} \approx -15$ kcal/mol in pure water to −30 kcal/mol in arabinose and −55 kcal/mol in glucuronate at the 0.1 mole fraction.

These results suggest that the presence of carboxylate groups in hemicellulose can strongly affect primary cell wall strength and raise two questions. (i) Is the strong stabilization effect of glucuronate due to the basic carboxylate group or the acidic hydronium ion? (ii) What is the contribution of the cyclic, sugar-like moiety of glucuronate? The 3D-RISM-KH calculations with an acetate anion as a basic hemicellulose branch model and a hydronium counterion indicate that the effect of acetate is modest and close to that of arabinose (Figure 1c). A comparison

dx.doi.org/10.1021/ja405634k | J. Am. Chem. Soc. 2013, 135, 19048−19051

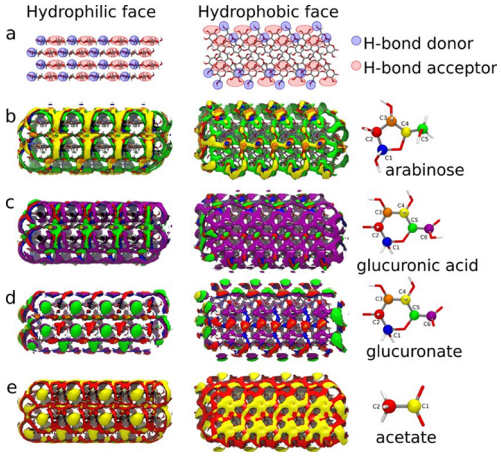

Figure 2. 3D site density distributions $g(\mathbf{r})$. (a) CN with highlighted hydrogen bond donor and acceptor sites. $g(\mathbf{r})$ of hemicellulose C atoms of (b) arabinose, (c) glucuronic acid, (d) glucuronate, and (e) acetate monomers around CN. Isosurfaces of $g(\mathbf{r}) = 1.4$ (except $g(\mathbf{r}) = 2.0$ for glucuronate C6 atom) are shown in the same colors as atoms.

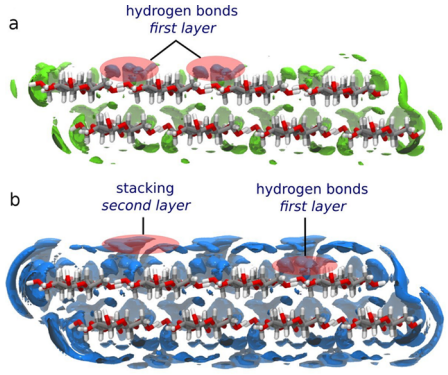

Figure 3. 3D solvation free energy density from glucuronate around CN. The larger negative isovalue (a, green) from highly localized distributions corresponds to hydrogen bonding. The smaller negative isovalue (b, blue) from a diffuse second layer corresponds to hemicellulose−cellulose stacking.

shows that the hydronium ions are not responsible for the strong effect observed for glucuronate, and about half of the effect comes from the sugar ring and the rest from the carboxylate group. In fact, the sum of ΔG_{agg} for acetate and arabinose is very close to ΔG_{agg} for glucuronate, suggesting that both the sugar and the basic functional group contribute to the stabilization of the cellulose fibril (gray line in Figure 1c and d). Finally, we note that ΔG_{agg} decreases almost linearly with hemicellulose concentration, which reflects the ability of hemicellulose branches to displace water molecules from the cellulose surface. These findings are fully consistent with the recent report of Mortimer et al.,[3] that preventing glucuronic acid (and hence glucuronate, depending on pH) incorporation in xylan branches yields plant cell walls more amenable to decomposition. Our results also explain the fact that NaOH removes hemicellulose from biomass.[30] A much stronger base, OH^- disrupts the glucuronate−cellulose interactions, thus destabilizing the cell wall microstructure. These findings might be used to design advanced biomass pretreatments.

Figure 2 gives the molecular picture of hemicellulose binding to the aggregated CNs in terms of the 3D spatial maps of density distributions of the representative sites (all C atoms) of hemicellulose branches. The cellulose surface H and O atoms available for hydrogen bonding are labeled as hydrogen bond donors and acceptors, respectively (Figure 2a). These maps (Figure 2b−e) indicate the regions of hemicellulose local density enhancement at the cellulose surface with respect to the hemicellulose bulk and allow reconstruction of preferred binding modes of hemicellulose branches around cellulose. The uncharged hemicellulose branches of arabinose and glucuronic acid interact with the cellulose hydrophilic faces mostly as hydrogen bond donors, e.g., by coordinating to available O atoms on the surface, whereas the glucuronate anions act as hydrogen bond acceptors by strongly interacting with the primary alcohol groups at the cellulose surface. Also, the distribution of acetate anions (Figure 2e) is similar to that of glucuronate anions, highlighting the importance of basic functional groups for coordination to hydroxyl groups. These results indicate that in plants, hemicellulose branches interact with the cellulose surface in a complementary fashion to stabilize the cell wall microstructure. The preferred orientation of hemicellulose branches over the hydrophobic surface is also determined by the polar interactions between the hemicellulose exocyclic group and the cellulose polar groups. The interaction of the endocyclic sites with the cellulose surface has a less specific, hydrophobic character, with no significant features on the distributions.

Figure 3 shows isosurfaces of the 3D spatial map of solvation free energy density (3D-SFED) coming from glucuronate at the cellulose surface. The entire solvation free energy μ_{solv} of the CNs immersed in hemicellulose hydrogel comprises 3D-SFED contributions $\Phi_s(\mathbf{r})$ from all hydrogel species s integrated over the solvation space: $\mu_{solv} = \sum_s \int d\mathbf{r}\, \Phi_s(\mathbf{r})$ (see Supporting Information, Methods). Further to 3D site density distributions, which provide solvation structure but present convolved information on interaction forces, the 3D-SFED maps explicitly characterize ensemble-averaged effective interactions of hemicellulose components spatially resolved over the cellulose surface, and thus unravel their effect on CN aggregation. The glucuronate 3D-SFED varies from large negative values for the most thermodynamically favorable arrangements of glucuronate at the cellulose surface to small negative values for less favorable arrangements. The larger negative value isosurface (Figure 3a) is highly localized around polar sites on the cellulose surface and indicates hydrogen bonding of hemicellulose to cellulose. The smaller negative value isosurface (Figure 3b) indicates a diffuse second layer of hemicellulose monomers stacking over the cellulose surface. The stacking interactions in the second layer are weaker and less specific than hydrogen bonding and are due to hydrophobic and enhanced intermolecular C−H···O interactions found in the cellulose X-ray structure.[31] Although the stacking interactions play a considerable role, the hemicellulose−cellulose binding is controlled mainly by the site-specific hydrogen bonds. The 3D-SFED maps of arabinose and glucuronic acid differ quantitatively, following the trends for ΔG_{agg} and PMF in Figure 1.

Significant advances have been achieved lately for comprehension of the cell wall inner architecture and its correlation with the enzymatic digestibility. Nonetheless, because of the high complexity of the cell wall, there is still a lack of molecular level characterization of these structures. Taking advantage of the 3D-RISM-KH molecular theory of solvation, we investigate, in a semiquantitative way, the effects of hemicellulose composition on the effective interactions with cellulose fibrils and show the substantial role of hemicellulose in the stability of the primary cell wall. Our approach reveals the relative contribution of different

dx.doi.org/10.1021/ja405634k | J. Am. Chem. Soc. 2013, 135, 19048−19051

xylan substitutions to cell wall strength and opens the opportunity to study the molecular basis of plant cell wall recalcitrance to an unprecedented level of detail by considering more elaborate cell wall models and including lignin into account. Our results show that the main effect of hemicellulose composition arises from the presence of basic groups but is not due to stereochemistry. Extending to other classes of hemicelluloses, such as galactoglucomannans, our results suggest that the effect of galactose, glucose and mannose would be rather weak and the largest contributions would arise from the carboxylate groups of random glucuronate substitutions. The PMF presented here can be measured using advanced nanoscale characterization techniques, such as surface force apparatus (SFA)[32] and atomic force microscopy.[4] For example, cellulose nanocrystals adsorbed on hydrophilic and hydrophobic surfaces of SFA placed in hemicellulose monomer hydrogels would provide the PMFs. Further, hydrogels containing hemicellulose oligomers and xylans with branches could be studied.

Recent approaches toward overcoming biomass recalcitrance involve genetic modification of crops to control lignin contents or composition and xylan structure so as to enable less severe pretreatment and efficient enzymatic processing.[3,33] Lignin extraction under mild conditions from transgenic plants is expected to enable enzyme access to the hydrophobic cellulose face while keeping the remaining cell wall structure intact with minimal alteration of the polysaccharides for effective digestion by enzymes.[4] We envision integrated biomass valorization based on extracting and decomposing the noncellulosic components to low molecular weight chemicals and utilizing the cellulose microfibrils to make nanocrystalline and nanofibrillar cellulose. These nanocellulosic materials are extensively manipulated to provide a rich suite of new materials and platforms for further transformations.[34,35] This is an important alternative to approaches of full conversion of lignocellulose to biofuels that face challenges arising from the deleterious impact of cellulose crystallinity on enzymatic processing.[36]

■ ASSOCIATED CONTENT

Supporting Information

Theoretical methods and additional results. This material is available free of charge via the Internet at http://pubs.acs.org.

■ AUTHOR INFORMATION

Corresponding Author

andriy.kovalenko@nrc-cnrc.gc.ca; skaf@iqm.unicamp.br

Notes

The authors declare no competing financial interest.

■ ACKNOWLEDGMENTS

This work is supported by the National Institute for Nanotechnology, University of Alberta, and the Research Foundation of the State of São Paulo FAPESP (CEPID 2013/08293-7). S.R.S. thanks Dr. John M. Villegas for discussion. The computations were performed on WestGrid−Compute/Calcul Canada.

■ REFERENCES

(1) Himmel, M. E.; Ding, S.; Johnson, D. K.; Adney, W. S.; Nimlos, M. R.; Brady, J. W.; Foust, T. D. *Science* **2007**, *315*, 804−807.

(2) Chundawat, S. P. S.; Beckham, G. T.; Himmel, M. E.; Dale, B. E. *Annu. Rev. Chem. Biomol. Eng.* **2011**, *2*, 121−145.

(3) Mortimer, J. C.; Miles, G. P.; Brown, D. M.; Zhang, Z.; Segura, M. P.; Weimar, T.; Yu, X.; Seffen, K. A.; Stephens, E.; Turner, S. R.; Dupree, P. *Proc. Natl. Acad. Sci. U. S. A.* **2010**, *107*, 17409−17414.

(4) Ding, S.-Y.; Liu, Y.-S.; Zeng, Y.; Himmel, M. E.; Baker, J. O.; Bayer, E. A. *Science* **2012**, *338*, 1055−1060.

(5) DeMartini, J. D.; Pattathil, S.; Miller, J. S.; Li, H.; Hahncde, M. G.; Wyman, C. E. *Energy Environ. Sci.* **2013**, *6*, 898−909.

(6) Beckham, G. T.; Matthews, J. F.; Peters, B.; Bomble, Y. J.; Himmel, M. E.; Crowley, M. F. *J. Phys. Chem. B* **2011**, *115*, 4118−4127.

(7) Payne, C. M.; Himmel, M. E.; Crowley, M. F.; Beckham, G. T. *J. Phys. Chem. Lett.* **2011**, *2*, 1546−1550.

(8) Linder, B.; Petridis, L.; Schulz, R.; Smith, J. C. *Biomacromolecules* **2013**, *14*, 3390−3398.

(9) Petridis, L.; Schulz, R.; Smith, J. C. *J. Am. Chem. Soc.* **2011**, *133*, 20277−20287.

(10) Kovalenko, A. In *Molecular Theory of Solvation*; Hirata, F., Ed.; Kluwer Academic: Dordrecht, The Netherlands, 2003; pp 169−275.

(11) Kovalenko, A.; Hirata, F. *J. Chem. Phys.* **1999**, *110*, 10095−10112.

(12) Kovalenko, A.; Hirata, F. *J. Chem. Phys.* **2000**, *112*, 10391−10417.

(13) Kovalenko, A. *Pure Appl. Chem.* **2013**, *85*, 159−199.

(14) Roman, M.; Cannizzo, C.; Pinault, T.; Isare, B.; Andrioletti, B.; van der Schoot, P.; Boutellier, L. *J. Am. Chem. Soc.* **2010**, *132*, 16818−16824.

(15) Aida, T.; Meijer, E. W.; Stupp, S. I. *Science* **2012**, *335*, 813−817.

(16) *Essentials of Glycobiology*, 2nd ed.; Varki, A., Cummings, R. D., Esko, J. D., Freeze, H. H., Stanley, P., Bertozzi, C., Hart, G. W., Etzler, M. E., Eds.; Cold Spring Harbor Laboratory Press: Cold Spring Harbor, NY, 2009.

(17) Dong, C.; Beis, K.; Nasper, J.; Brunkan-LaMontagne, A. L.; Clarke, B. R.; Whitfield, C.; Naismith, J. H. *Nature* **2006**, *444*, 226−229.

(18) Gama, C. I.; Tully, S. E.; Sotogaku, N.; Clark, P. M.; Pawat, M.; Vaidehi, N.; Goddard, W. A., III; Nishi, A.; Hsieh-Wilson, L. C. *Nat. Chem. Biol.* **2006**, *2*, 467−473.

(19) Pauly, M.; Keegstra, M. *Plant J.* **2008**, *54*, 559−568.

(20) Cho, H. M.; Gross, A. S.; Chu, J.-W. *J. Am. Chem. Soc.* **2011**, *133*, 14033−14041.

(21) Stumpe, M. C.; Blinov, N.; Wishart, D.; Kovalenko, A.; Pande, V. S. *J. Phys. Chem. B* **2011**, *115*, 319−328.

(22) Johnson, R. S.; Yamazaki, T.; Kovalenko, A.; Fenniri, H. *J. Am. Chem. Soc.* **2007**, *129*, 5735−5743.

(23) Yamazaki, T.; Fenniri, H.; Kovalenko, A. *ChemPhysChem* **2010**, *11*, 361−367.

(24) Kovalenko, A.; Kobryn, A. E.; Gusarov, S.; Lyubimova, O.; Liu, X.; Blinov, N.; Yoshida, M. *Soft Matter* **2012**, *8*, 1508−1520.

(25) Fafard, J.; Lyubimova, O.; Stoyanov, S. R.; Dedzo, G. K.; Gusarov, S.; Kovalenko, A.; Detellier, C. *J. Phys. Chem. C* **2013**, *117*, 18556−18566.

(26) Yoshida, N.; Phongphanphanee, S.; Maruyama, Y.; Imai, T.; Hirata, F. *J. Am. Chem. Soc.* **2006**, *128*, 12042−12043.

(27) Phongphanphanee, S.; Yoshida, N.; Hirata, F. *J. Am. Chem. Soc.* **2008**, *130*, 1540−1541.

(28) Yoshida, N.; Imai, T.; Phongphanphanee, S.; Kovalenko, A.; Hirata, F. *J. Phys. Chem. B* **2009**, *113*, 873−886.

(29) Gomes, T. C. F.; Skaf, M. S. *J. Comput. Chem.* **2012**, *33*, 1338−1346.

(30) Agbor, V. B.; Cicek, N.; Sparling, R.; Berlin, A.; Levin, D. B. *Biotechnol. Adv.* **2011**, *29*, 675−685.

(31) Nishiyama, Y.; Sugiyama, J.; Chanzy, H.; Langan, P. *J. Am. Chem. Soc.* **2003**, *125*, 14300−14306.

(32) Maeda, N.; Chen, N.; Tirrell, M.; Israelachvili, J. *Science* **2002**, *297*, 379−382.

(33) Chen, F.; Dixon, R. A. *Nat. Biotechnol.* **2007**, *25*, 759−761.

(34) Habibi, Y.; Lucia, L. A.; Rojas, O. J. *Chem. Rev.* **2010**, *110*, 3479−3500.

(35) Nogi, M.; Iwamoto, S.; Nakagaito, A. N.; Yano, H. *Adv. Mater.* **2009**, *21*, 1595−1598.

(36) Chundawat, S. P. S.; Bellesia, G.; Uppugundla, N.; da Costa Sousa, L.; Gao, D.; Cheh, A. M.; Agarwal, U. P.; Bianchetti, C. M.; Phillips, G. N.; Langan, P.; Balan, V.; Gnanakaran, S.; Dale, B. E. *J. Am. Chem. Soc.* **2011**, *133*, 11163−11174.